Proceedings of the
Annual Stability Conference
Structural Stability Research Council
Atlanta, Georgia, April 21-24, 2026

Stability of high-strength SpeedCore walls: evaluation of AISC slenderness limit

Tariq Sweidan[1], Morgan Broberg[2]

Abstract

Composite plate shear walls, also called SpeedCore, consist of two parallel steel faceplates connected with tie bars and filled with concrete. The steel faceplates serve as the longitudinal reinforcement of the wall and as permanent formwork for the concrete. SpeedCore is an attractive system because it has similar strength and stiffness compared to conventional reinforced concrete walls, but takes 40% less onsite construction time. To achieve this behavior a limit on plate slenderness is enforced. This limit is intended to prevent premature local buckling of the steel faceplates of the composite section. Local buckling depends on several parameters such as steel plate thickness, tie bar or shear stud spacing, and the strength of steel. This limit is based on existing experiments and analysis of normal strength steel (yield strength of 36 to 50 ksi). This paper investigates the axial behavior of SpeedCore walls with high strength steel (up to 100 ksi) using benchmarked finite element approach. Twenty specimens with varying steel yield strength and slenderness ratio were analyzed, including the effect of initial imperfections. The analysis indicates that for a given faceplate thickness, increasing tie bar spacing reduces axial capacity, while higher faceplate yield strength increases axial capacity. The current AISC design classification and design equations, including faceplate slenderness limit, were developed for conventional strength steel walls and do not fully capture the influence of tie bar spacing and high strength steel, leading to unconservative predictions.

1. Introduction

Composite plate shear walls (C-PSW), also called SpeedCore, are a structural system developed to accelerate construction schedules without compromising structural performance or lateral resistance. The system consists of two parallel steel faceplates connected with tie bars and filled with concrete. The steel faceplates eliminate the need for formwork and serve as the longitudinal reinforcement of the wall. This reduces the onsite labor and accelerates the construction schedules as it takes 40% less construction time compared to conventional reinforced concrete walls (Klemencic 2019).

In the light of these advantages, there has been growing interest in using SpeedCore walls in medium to high-rise buildings, and increased research on their structural behavior. Most

[1] Graduate Research Assistant, University of Arkansas, <tsweidan@uark.edu>
[2] Assistant Professor, University of Arkansas, <mbroberg@uark.edu>

SpeedCore research and applications use conventional steel grades, typically ASTM A36 Grade 36 and ASTM A572 Grade 50. The current AISC Specification limits the yield strength to a maximum of 75 ksi and do not provide any recommendations for using high strength steel in SpeedCore walls (AISC 360, 2022). Meanwhile, steel manufacturers have developed high-strength steels with yield strengths exceeding 100 ksi, potentially allowing thinner and lighter SpeedCore walls. However, investigations have been limited for high strength SpeedCore walls including the axial capacity, faceplate local buckling and post buckling response. Addressing these gaps is essential for advancing the economic use of this system. This paper investigates the axial behavior of SpeedCore walls made from high strength steel and compares this performance to conventional strength steel using benchmarked 3D finite element approaches.

2. Background

Experimental research on the axial compression strength of high strength SpeedCore walls is limited. The current AISC slenderness equation I1-4 (AISC 360, 2022), was developed based on the testing performed by Zhang et al. (2020; 2014). The 2020 Zhang et al. study showed that the shear stud spacing to plate thickness ratio controls whether the faceplates buckle elastically or inelastically, and if plate yielding or local buckling controls the wall strength (2020). Three recent studies have included high strength steels (Mo et al. 2022; Yao et al. 2025; Wang et al. 2024). Mo et al. tested ten high strength composite walls with yield strength up to 150 ksi using S690 and S960 steel plates (2022). The walls had a constant size of (16 in. x 24 in. x 5.5 in.) with either tie bars or shear studs. Their results showed that walls with non-slender faceplates can develop yielding before local buckling, while walls with slender plates buckle in the elastic range (2022). Yao et al. conducted axial compression tests on ten high strength SpeedCore walls with yield strength up to 110 ksi, all with constant dimensions of (14 in. x 11 in. x 5 in.) with both headed studs and tie bars (2025). Their results showed that the axial strength of SpeedCore walls increase with increasing material strength and decreasing slenderness ratio (2025). Wang et al. tested eighteen composite walls specimens all with dimensions of (14 in. x 11 in. x 5 in.) using both shear studs and tie bars (2024). One faceplate is made with Q690 high strength steel with a yield strength of 100 ksi, and the other faceplate is made of stainless clad steel with a yield strength of 50 ksi and ultra-high-performance concrete infill. Their results showed that stud spacing to plate thickness ratio strongly affects the strength and local buckling of the walls (2024).

3. Modeling Approach

Benchmarked 3D finite element models were developed using Abaqus (Abaqus 2025). The concrete infill, the steel faceplates, and the tie bars were all modeled using eight node solid elements with reduced integration (C3D8R). All steel components were merged into one part, consistent with welding between steel tie bars and faceplate. Typical steel and concrete parts are shown in Figure 1(a). Interaction was modeled using the general contact, tangential behavior was defined using coulomb friction coefficient of 0.5, and the normal behavior was modeled with hard contact. A global mesh size of 0.6 in. was used for the concrete infill, and 0.3 in. for both the steel plates and tie bars, with two elements through thickness in the steel faceplates as shown Figure 1(b). This mesh scheme was confirmed through a mesh sensitivity analysis.

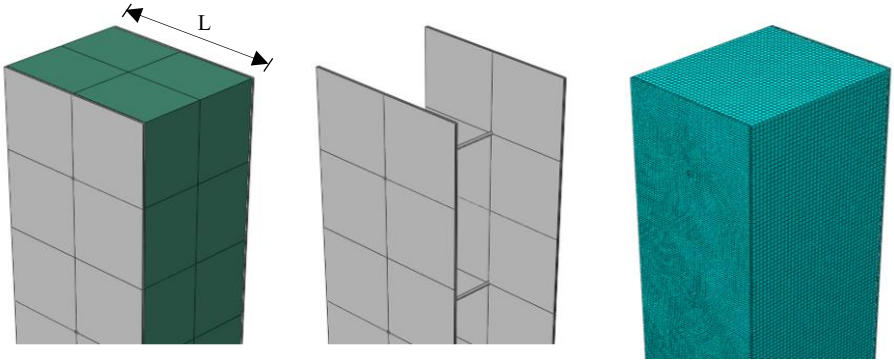

(a) (b)

Figure 1: (a) Typical Steel and Concrete Parts (b) Meshed Parts (where L is the wall length)

The concrete material behavior was modeled using the concrete damaged plasticity (CDP) model. The CDP parameters were defined as follows: dilation angle = 25°, eccentricity = 0.1, $f_{b0}/f_c' = 1.16$, $k_c = 0.667$ and viscosity parameter = 0. These parameters are consistent with the model proposed by Tao et al. (2013).

The steel material behavior was modeled using a power law model following Eq. (1). The resulting true stress-plastic strain data were implemented in Abaqus.

$$\sigma = \begin{cases} E * \varepsilon, & \varepsilon \leq \dfrac{\sigma_y}{E} \\ \sigma_y, & \dfrac{\sigma_y}{E} < \varepsilon \leq \varepsilon_{sh} \\ \sigma_u - (\sigma_u - \sigma_y)\left(\dfrac{\varepsilon_u - \varepsilon}{\varepsilon_u - \varepsilon_{sh}}\right)^n, & \varepsilon > \varepsilon_{sh} \end{cases} \quad (1)$$

Where E is the modulus of elasticity, σ_y is the yield stress, σ_u is the ultimate stress, ε_{sh} is the strain at the strain hardening, ε_u is the strain at ultimate.

The walls were fixed at the base and pinned at the top. Displacement-controlled axial shortening was applied to a reference point on the top of the wall, with a maximum displacement of 0.5 in.

Initial imperfections in the steel faceplates were considered in the modeling approach. Buckling analysis was conducted on the steel modules, and the resulting buckling shapes with outward local buckling between the tie bars were selected to define the initial imperfections. Values of initial imperfections from $0.1t_p$ to $0.5t_p$ were considered. An imperfection magnitude of $0.1t_p$ was chosen because it resulted in the closest agreement with experimental results.

This approach is conservative since the initial imperfections are of the same shape as the expected plate local buckling. The magnitude is consistent with the faceplate waviness limit specified in AISC N690 (2024) and shown in Eq. (2). A representative buckling shape is shown in Figure 2.

$$f_w \leq \left(\frac{t_p}{2}\right)\left(\frac{s_{t,min}}{s}\right) \quad (2)$$

Where f_w is the faceplate waviness, s is the spacing of steel anchors, $s_{t,min}$ is the minimum tie spacing and t_p is the thickness of faceplate.

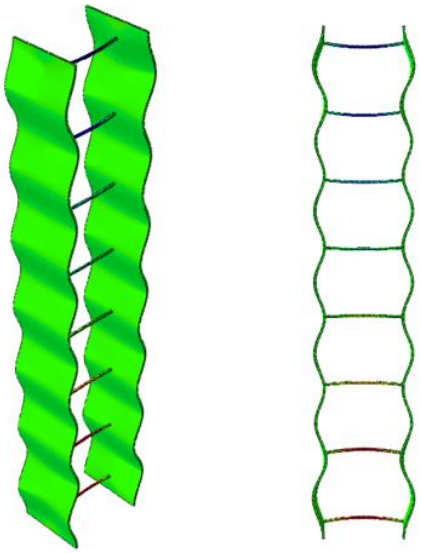

Figure 2: Buckling Mode (amplified)

The finite element modeling approach was benchmarked using the experimental test data reported in (Mo et al. 2022). Three specimens, N-CW-40-QB, H-CW-32-QB, and H-CW-19.2-QB were used for benchmarked modeling. N-CW-40-QB was made from conventional strength steel (yield strength of 40 ksi) while H-CW-32-QB, and H-CW-19.2-QB were made from high strength steel (yield strength of 110 ksi). N-CW-40-QB and H-CW-32-QB are slender walls with slenderness ratio of 40 and 32 respectively, while H-CW-19.2-QB is non-slender wall with slenderness ratio of 19.2, per AISC equation I1-4 (AISC 360, 2022). All specimens have dimensions of (16 in. x 24 in. x 5.5 in.) and include only tie bars.

The load-displacement curves from the Abaqus models in Figure 3, showed good agreement with the experimental results, and the initial stiffness followed the experimental trend. Both N-CW-40-QB and H-CW-32-QB specimens experienced local buckling in the steel faceplates prior to yielding, while specimen H-CW-19.2-QB experienced yielding before local buckling. The ultimate load of specimen N-CW-40-QB from Abaqus was 425 kips compared to 445 kips recorded in the test (4.5% difference). For specimen H-CW-32-QB the ultimate load from Abaqus was 662 kips, while the test result was 678 kips (2.4% difference). For specimen H-CW-19.2-QB the ultimate load from Abaqus was 854 kips, while the test result was 914 kips (6.5% difference).

The model post-peak behavior was conservative for N-CW-40-QB. The post-peak behavior is sensitive to initial imperfection assumptions; the modeling approach assumes initial imperfections of $0.1t_p$ located according to the buckling mode. This approach is inherently conservative since the greatest imperfection is at the most punishing location. Initial imperfection magnitude and variation across the cross-section were not reported by the authors. Moreover, initial imperfection for in-service walls would only be checked against allowable tolerances. In this study, the post-

peak behavior is not of concern because this paper focuses on the failure mode and compression capacity of SpeedCore walls.

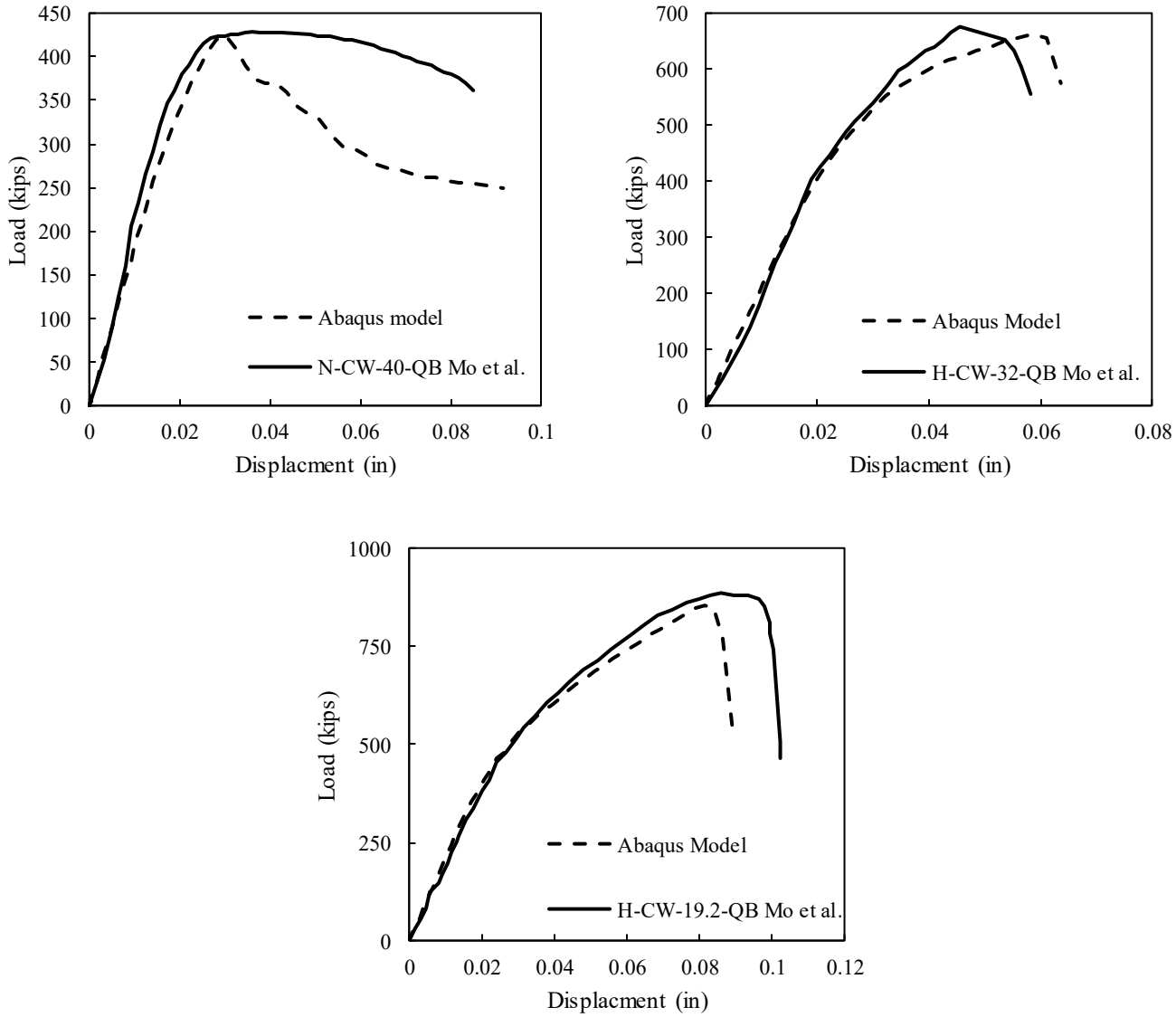

Figure 3: Load-Displacement Curves of the Benchmarked Models

4. Finite Element Models

A total of 20 models were developed to study the influence of steel faceplate strength and plate slenderness. The study parameters were the steel plate yield strength (F_y) and slenderness ratio (s/t_p). These parameters were selected as both directly influence the local buckling of steel faceplates in SpeedCore walls. The specimens were divided into four groups based on the yield strength of the steel faceplates, each group consists of five specimens, and each specimen represents a different steel plate slenderness ratio. The height (H), wall thickness (t_{sc}), steel faceplate thickness (t_p) and tie bar diameter were 150 in., 24 in., 0.5 in., and 0.75 in., respectively. These values were consistent across all specimens. The length (L) varied but was equal to the tie

bars spacing (s). This approach isolated one SpeedCore cell consisting of one tie bar, and half the tie spacing on either side (see Figure 1(a)). Within each group, the tie bar spacings were 10 in., 12 in., 15 in., 20 in., and 30 in., which results in s/t_p ratio ranging from 20 to 60. This range of slenderness values captures sections that meet the AISC slenderness requirement and those that do not. Table 1 summarizes the models details, the model ID indicates the tie bar spacing, and the faceplate yield strength. For example, SC-10-36 refers to a SpeedCore wall with a 10 in. tie bar spacing and a 36 ksi steel faceplates yield strength.

Table 1: Finite Element Models Details

Group	Model ID	s in	F_y ksi	t_p in	s/t_p	AISC Slenderness Limit[1]	H in	L in	t_{sc} in	f'_c ksi
1	SC-10-36	10	36	0.50	20	34.1	150	10	24	10
	SC-12-36	12	36	0.50	24	34.1	150	12	24	10
	SC-15-36	15	36	0.50	30	34.1	150	15	24	10
	SC-20-36	20	36	0.50	40	34.1	150	20	24	10
	SC-30-36	30	36	0.50	60	34.1	150	30	24	10
2	SC-10-50	10	50	0.50	20	28.9	150	10	24	10
	SC-12-50	12	50	0.50	24	28.9	150	12	24	10
	SC-15-50	15	50	0.50	30	28.9	150	15	24	10
	SC-20-50	20	50	0.50	40	28.9	150	20	24	10
	SC-30-50	30	50	0.50	60	28.9	150	30	24	10
3	SC-10-80	10	80	0.50	20	22.8	150	10	24	10
	SC-12-80	12	80	0.50	24	22.8	150	12	24	10
	SC-15-80	15	80	0.50	30	22.8	150	15	24	10
	SC-20-80	20	80	0.50	40	22.8	150	20	24	10
	SC-30-80	30	80	0.50	60	22.8	150	30	24	10
4	SC-10-100	10	100	0.50	20	20.4	150	10	24	10
	SC-12-100	12	100	0.50	24	20.4	150	12	24	10
	SC-15-100	15	100	0.50	30	20.4	150	15	24	10
	SC-20-100	20	100	0.50	40	20.4	150	20	24	10
	SC-30-100	30	100	0.50	60	20.4	150	30	24	10

[1]Slenderness Limit = $1.2 * \sqrt{\frac{E}{F_y}}$ (AISC 360, 2022)

5. Material Models

Four grades of steel were considered in the numerical models: ASTM A36 Grade 36, ASTM A572 Grade 50, ASTM A1066 Grade 80 and ASTM A514 Grade 100. The values of the yield and ultimate stress were based on the relevant ASTM standards. Yield plateau, ultimate strain, and the power law coefficient were selected based on published experimental coupon tests: ASTM A36 and ASTM A572 (Sajid and Kiran 2018), ASTM A514 (Partin et al. 2010) and S500MC (Wang et al., 2017). Due to the lack of published experimental data on ASTM A1066 Grade 80, the

S500MC was adopted as it has similar mechanical properties. Based on these studies, the ultimate strain (ε_u) was assumed to be 0.25 in/in for grades 36 and 50, and 0.12 in/in for grades 80 and 100, and the power law coefficient (n) was set to 5. High strength steel typically shows a short or absent yield plateau compared to conventional strength steel, which is due to the differences in microstructure and processing that limit yielding and results in smoother transition from elastic to plastic behavior. The engineering and true stress-strain relationships are shown in Figure 4(a) and Table 2 summarizes the adopted mechanical properties of the steel plates.

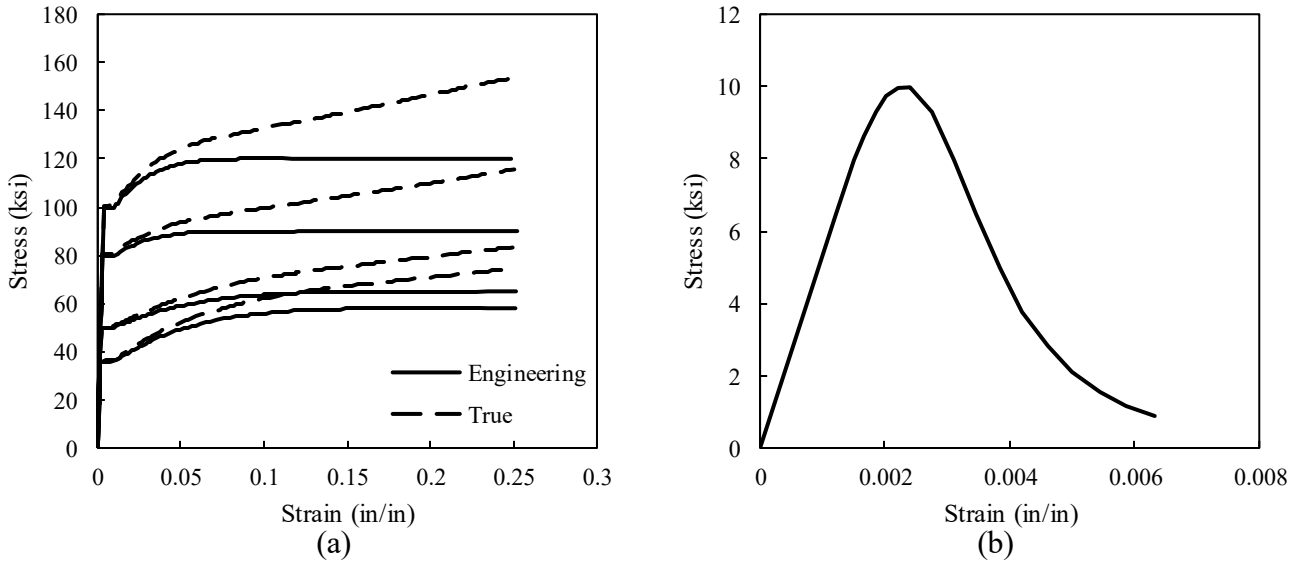

Figure 4: Stress-Strain Curves (a) Steel (b) Concrete

Table 2: Steel Mechanical Properties

Grade	E	F_y	F_u	ε_u
	ksi	ksi	ksi	in/in
ASTM A36	29000	36	58	0.25
ASTM A572 Gr. 50	29000	50	65	0.25
ASTM A1066 Gr. 80	29000	80	90	0.12
ASTM A514 Gr. 100	29000	100	120	0.12

A concrete compressive strength (f'_c) of 10 ksi was used for the concrete infill. The stress-strain curve is shown in Figure 4(b). One concrete compressive strength was considered in the analysis as the focus of this study is the steel faceplate buckling behavior, and the variation in concrete strength has a negligible influence on the steel plates buckling.

6. Initial Imperfections

The inclusion of initial imperfections primarily affected the ultimate axial strength of the models, while the failure mode and local buckling of steel faceplates remained unchanged. As shown in Figure 5, the ultimate axial capacity decreased from 2732 kips/ft for the model without imperfections to 2612 kips/ft after introducing a $0.1t_p$ imperfection magnitude (4% difference). A further reduction in ultimate strength was observed after introducing a $0.3t_p$ imperfection magnitude, with ultimate axil capacity of 2420 kips/ft (11% difference compared to the no imperfections model). Also, increasing the imperfection magnitude to $0.5t_p$ resulted in decrease in capacity to 2406 kips/ft (12% difference compared to the no imperfections model). This reduction in axial capacity occurs because initial imperfections introduce earlier stress concentrations, which accelerate instability and reduce the peak load the wall can carry. An initial imperfection magnitude of $0.1t_p$ was adopted in this study, as during the benchmarking, $0.1t_p$ resulted in the closest agreement with the experimental results.

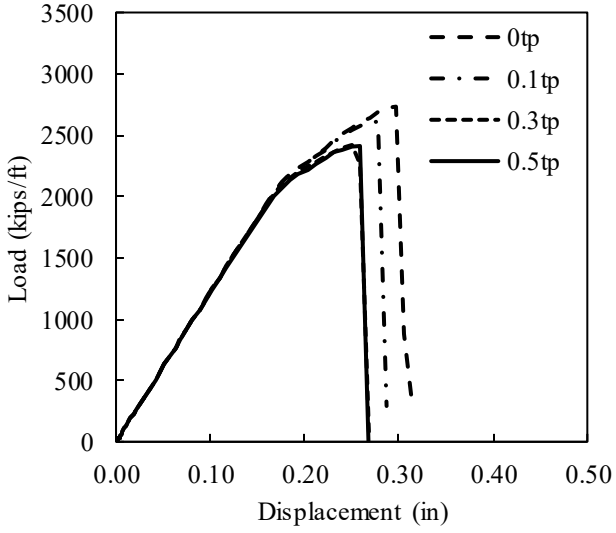

Figure 5: Effect of Initial Imperfections on Specimen SC-10-36

7. Results and Discussion

For each model, the load-displacement curve and the peak axial load were extracted. These results were compared to the nominal design axial strength, computed using the design equations in (AISC 360, 2022). Table 3 summarizes the normalized FEM (P_{FEM}) and computed (P_{AISC}) peak strengths. The final column represents the percent reduction in the normalized FEM peak strength relative to the smallest tie bar spacing (10 in.) within each group. This value is intended to quantify the impact that greater tie spacing (and therefore less ties) has on the ultimate strength.

Table 3: Models Results

Group	Model ID	s/t_p	AISC Slenderness Limit	P_{FEM} kips/ft	P_{AISC} kips/ft	P_{FEM}/P_{AISC}	%Reduction[1]
1	SC-10-36	20	34.1	2612.3	2695.9	0.97	-
	SC-12-36	24	34.1	2435.1	2695.9	0.90	6.8
	SC-15-36	30	34.1	2417.0	2695.9	0.90	7.5
	SC-20-36	40	34.1	2339.9	2695.9	0.87	10.4
	SC-30-36	60	34.1	2157.9	2695.9	0.80	17.4
2	SC-10-50	20	28.9	2872.6	2853.7	1.01	-
	SC-12-50	24	28.9	2828.2	2853.7	0.99	1.5
	SC-15-50	30	28.9	2859.5	2853.7	1.00	0.5
	SC-20-50	40	28.9	2634.7	2853.7	0.92	8.3
	SC-30-50	60	28.9	2246.1	2853.7	0.79	21.8
3	SC-10-80	20	22.8	3033.1	3190.0	0.95	-
	SC-12-80	24	22.8	2885.0	3190.0	0.90	4.9
	SC-15-80	30	22.8	2985.6	3190.0	0.94	1.6
	SC-20-80	40	22.8	2765.9	3190.0	0.87	8.8
	SC-30-80	60	22.8	2299.4	3190.0	0.72	24.2
4	SC-10-100	20	20.4	3029.5	3412.8	0.89	-
	SC-12-100	24	20.4	2886.4	3412.8	0.85	4.7
	SC-15-100	30	20.4	2987.0	3412.8	0.88	1.4
	SC-20-100	40	20.4	2771.0	3412.8	0.81	8.5
	SC-30-100	60	20.4	2299.4	3412.8	0.67	24.1

[1]%Reduction= $\frac{P_{FEM}-P_{FEM,10in}}{P_{FEM,10in}} * 100$

The load-displacement curves in Figure 6 showed a reduction in the axial capacity as the tie bar spacing increased from 10 in. to 30 in. (s/t_p from 20 to 60) across all yield strengths. The reduction in axial capacity shown in Table 3 ranged from 17.4% for the yield strength 36 ksi, up to 24.1% for the yield strength 100 ksi. For a given plate thickness, increasing the tie bar spacing decreases the axial capacity of SpeedCore walls regardless of the faceplate yield strength. Also, the failure modes in Figure 7 show that increasing the tie bar spacing for a given plate thickness results in an increased faceplate unbraced length. In turn, this greater unbraced length results in a reduction in their buckling resistance and increase in out of plane deflection.

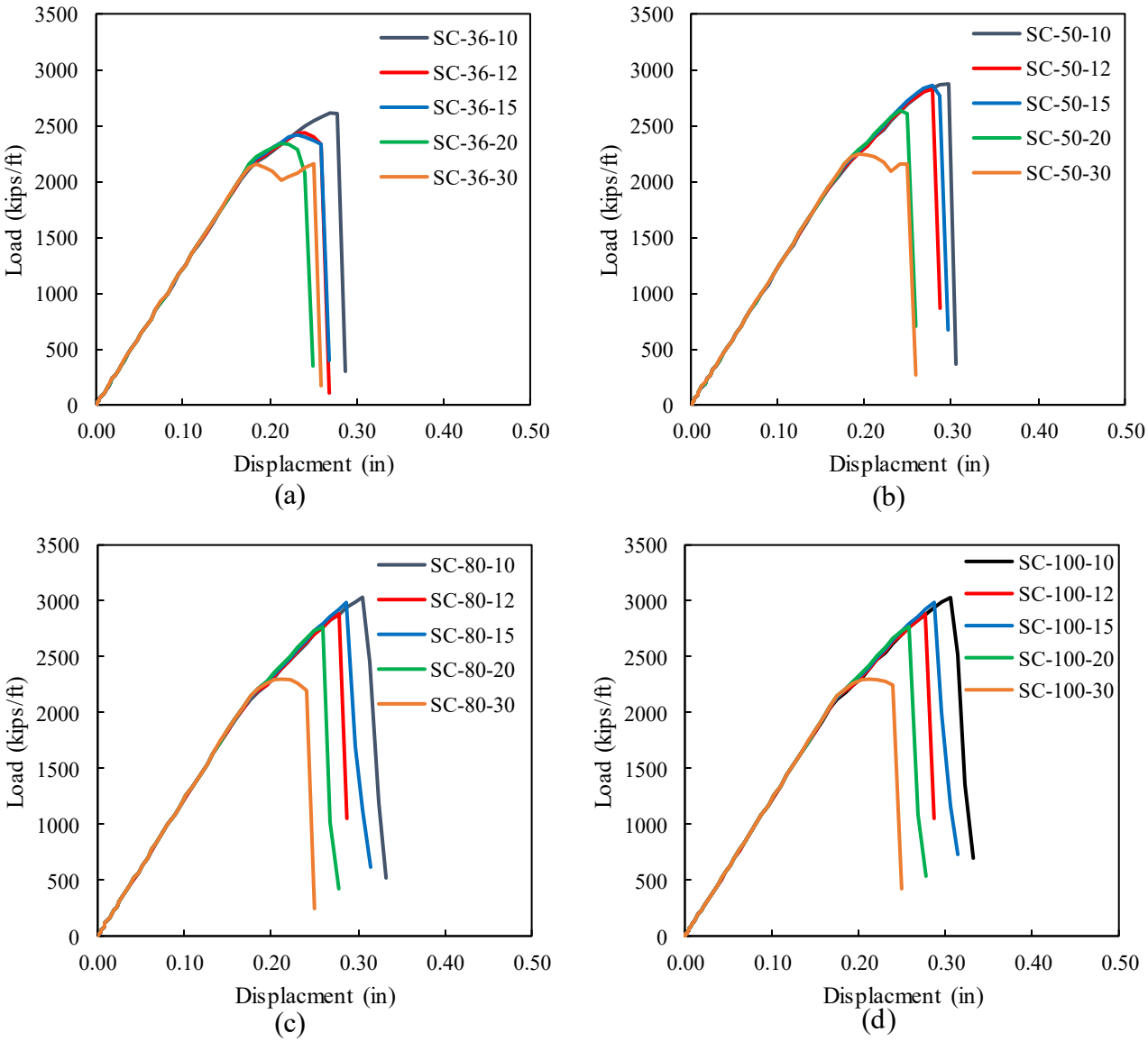

Figure 6: Effect of Tie Bar Spacing on Load-Displacement Curves (a) 36 ksi (b) 50 ksi (c) 80 ksi (d) 100 ksi

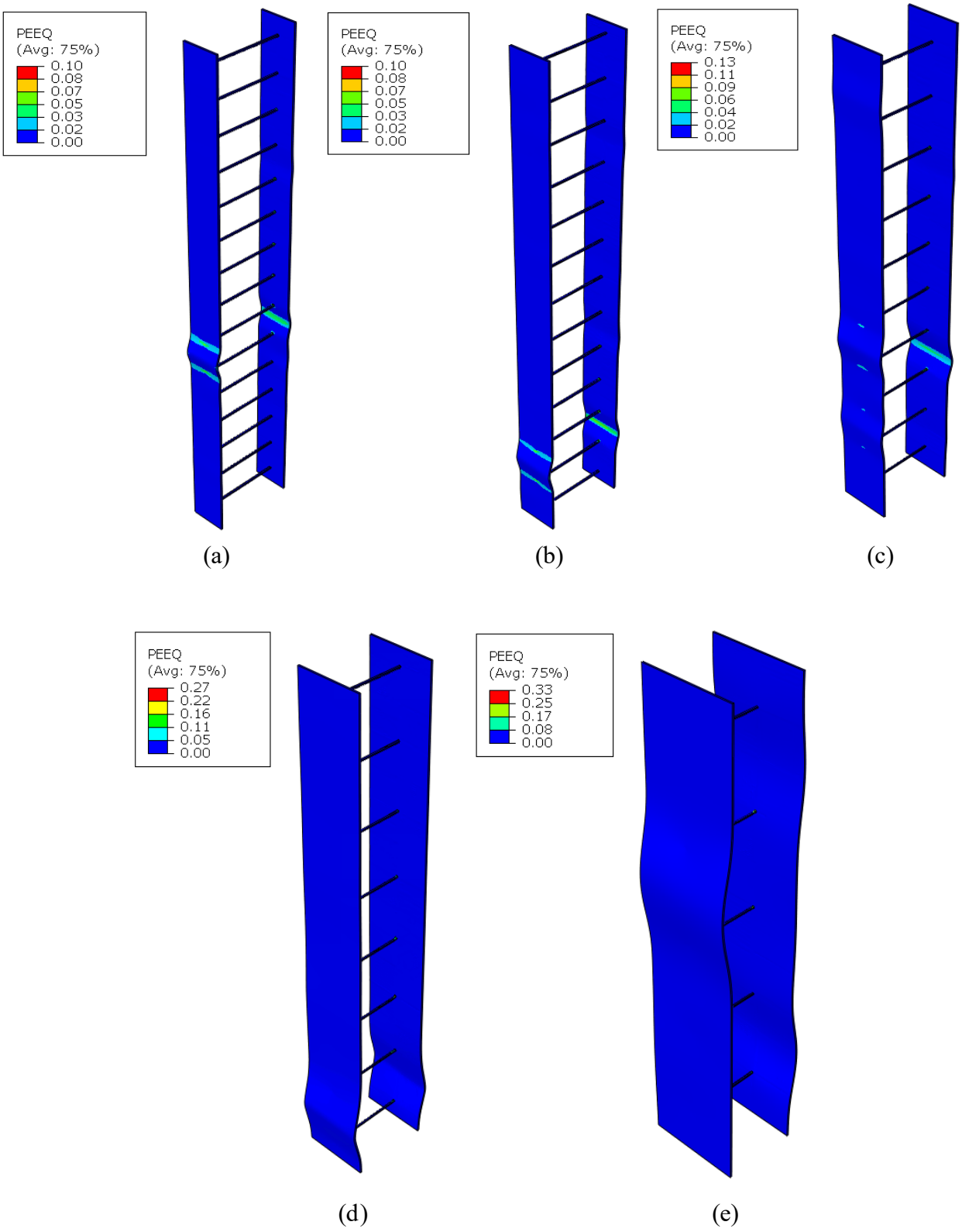

Figure 7:Local Buckling of Specimens (a) SC-36-10 (b) SC-50-12 (c) SC-50-15 (d) SC-80-20 (e) SC-100-30

The comparison between the FEM capacity and the AISC calculated strengths shows that for the given plate thickness the AISC equation provides a better prediction of the axial capacity when the tie bar spacing is small (less than 15 in. or s/t_p of 30).

For specimens that meet the AISC slenderness limit, the ratio of the FEM capacity to the AISC capacity was 0.90 to 0.97 for 36 ksi steel, 0.99 to 1.01 for 50 ksi steel, 0.95 for 80 ksi steel and 0.89 for 100 ksi steel. For specimens that did not meet the slenderness limit it showed lower ratios, with values ranging from 0.80 to 0.87 for 36 ksi steel, 0.79 to 1.0 for 50 ksi steel, 0.72 to 0.94 for 80 ksi steel, and 0.67 to 0.88 for 100 ksi steel. The reduction in the FEM capacity to the AISC capacity ratio becomes more pronounced with increasing steel plate strength, indicating that the AISC design equation is overpredicting the axial capacity, especially for SpeedCore walls with high-strength plates. This overprediction is in part because the AISC does not account for the influence of the tie bar spacing in the axial design equation. Instead, tie bar spacing is considered through the ratio s/t_p and the faceplate slenderness limit, which classifies walls as slender or non-slender and works as an acceptability criterion. This analysis also shows that plate grade has an impact on this overprediction.

The influence of the steel yield strength on the axial capacity was reflected in the FEM results across all slenderness ratios. Figure 8(a) shows that for specimens with 10 in. tie bar spacing, increasing the steel yield strength from 36 ksi to 100 ksi, results in a clear increase in the axial capacity, which increased from 2612.3 kips/ft to 3029.5 kips/ft (15.9% increase). A similar trend is observed in Figure 8(b) for specimens with 20 in. tie bar spacing, where the axial capacity increased from 2339.9 kips/ft at 36 ksi up to 2771 kips/ft at 100 ksi (18.4% increase). These results showed that higher strength steel could carry more axial load before reaching its yield point and before local buckling becomes critical, despite the s/t_p ratio exceeding the slenderness limit. Overall, using high strength steel improves the axial capacity of SpeedCore walls.

All FEM specimens exhibited local buckling of steel faceplates, but the behavioral patterns were different. In specimens with small spacing, less than 15 in. (s/t_p less than 30), local buckling occurred after yielding in the steel faceplates. In specimens with large spacing, greater than 15 in. (s/t_p greater than 30), local buckling occurred at lower load level before steel yielding. In other words, for a given plate thickness, closer tie bars delay plate instability and allow the steel faceplates to reach higher stress before local buckling. In contrast, specimens with larger tie bar spacings exhibit earlier local buckling and reduction in overall axial capacity. This behavior is seen regardless of steel faceplate yield strength.

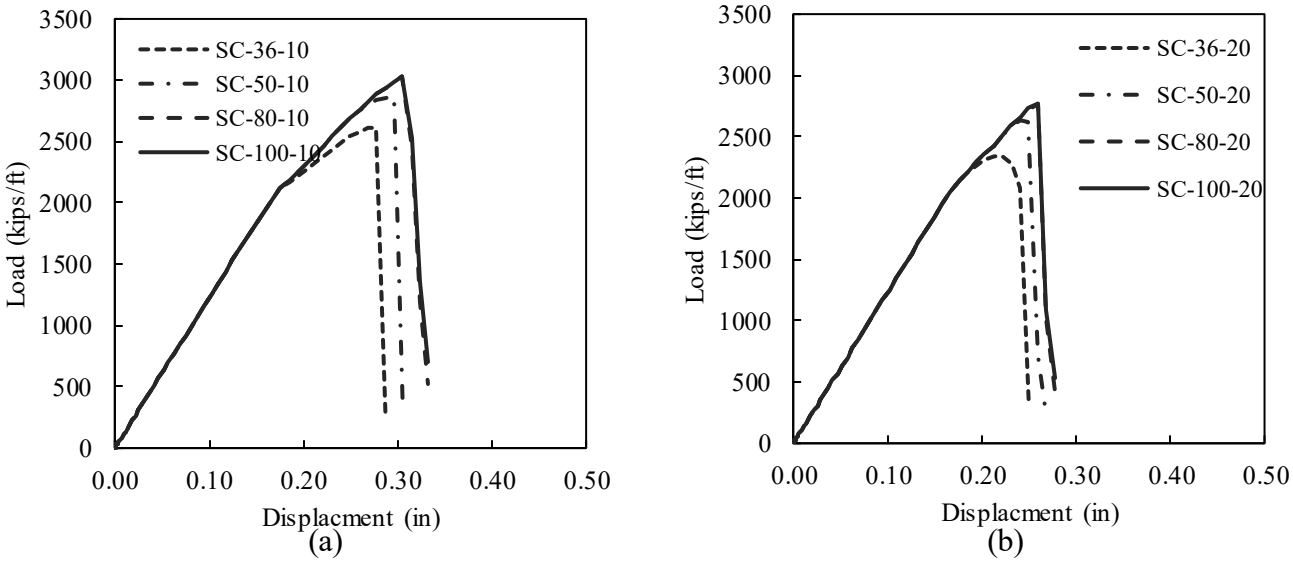

Figure 8: Effect of Steel Faceplate Yield Strength on Load-Displacement Curves (a) 10 in. (b) 20 in.

8. Conclusions

This paper investigated the axial compression behavior of SpeedCore walls using benchmarked 3D finite element analysis. A total of twenty specimens with varying steel faceplate strength and slenderness ratios were investigated. The FEM results showed that for a given plate thickness, increasing the tie bar spacing significantly reduces the axial capacity of the SpeedCore wall regardless of the faceplate yield strength. Also, increasing the yield strength from 36 ksi to 100 ksi showed a noticeable improvement in axial capacity.

The investigation showed a limitation in the AISC classification for high strength steel walls. This limitation is because AISC classifies SpeedCore walls as non-slender or slender based on the s/t_p ratio and the slenderness limit. This classification works reasonably for conventional strength steel, but it becomes less accurate for high strength steel such as 80 ksi and 100 ksi. Based on this classification, increasing the steel strength can cause walls with the same slenderness ratio to be classified from non-slender to slender, despite exhibiting local buckling behavior comparable to non-slender walls. The results also showed that the AISC design equation, which does not account for wall slenderness, may unnecessarily penalize walls with slender plates that exhibit strengths comparable to non-slender walls. This shows a limitation in the current slenderness limit and suggests that a revised wall capacity equation accounting for both slender and non-slender walls could be beneficial. Such an equation could be especially beneficial for deflection-governed systems where stiffness, not strength, is the primary design variable since tie spacing could be stretched beyond the current limit without compromising system safety.

Additional experimental and numerical studies are recommended to better understand the axial behavior of SpeedCore walls made with high strength steel. Research should investigate the influence of faceplate thickness, slenderness ratio, and the effect of the actual versus specified yield strength on the wall capacity and failure modes. Future research should also evaluate the second tie bar spacing limit (AISC Equation I1-5) enforced for constructability. Such research would support the development of an improved design equation that accounts for tie bar spacing and high strength steel, providing more accurate predictions.

References

Dassault Systemes Simulia Corp. 2025. Abaqus. V. 2025. Released. https://www.3ds.com/products/simulia/abaqus.

Klemencic, Ron. 2019. "Learn All About SpeedCore at NASCC: The Steel Conference." American Institute of Steel Construction (AISC). https://www.aisc.org/modern-steel/news/learn-all-about-speedcore-at-nascc-the-steel-conference/.

Mo, Jun, Brian Uy, Dongxu Li, Huu-Tai Thai, and Youtian Wang. 2022. "Behaviour and Design of Composite Walls under Axial Compression." Journal of Constructional Steel Research 199 (December): 107635. https://doi.org/10.1016/j.jcsr.2022.107635.

Partin, K., K.O. Findley, and C.J. Van Tyne. 2010. "Microstructural and Alloy Influence on the Low-Temperature Strengthening Behavior of Commercial Steels Used as Plates." Materials Science and Engineering: A 527 (20): 5143–52. https://doi.org/10.1016/j.msea.2010.04.092.

Sajid, Hizb Ullah, and Ravi Kiran. 2018. "Influence of High Stress Triaxiality on Mechanical Strength of ASTM A36, ASTM A572 and ASTM A992 Steels." Construction and Building Materials 176 (July): 129–34. https://doi.org/10.1016/j.conbuildmat.2018.05.018.

Specification for Safety-Related Steel Structures for Nuclear Facilities. 2024. ANSI/AISC N690-24. American Institute of Steel Construction.

Specification for Structural Steel Buildings (ANSI/AISC 360-22). 2022. ANSI/AISC 360-22. American Institute of Steel Construction.

Tao, Zhong, Zhi-Bin Wang, and Qing Yu. 2013. "Finite Element Modelling of Concrete-Filled Steel Stub Columns under Axial Compression." Journal of Constructional Steel Research 89 (October): 121–31. https://doi.org/10.1016/j.jcsr.2013.07.001.

Wang, J., S. Afshan, N. Schillo, M. Theofanous, M. Feldmann, and L. Gardner. 2017. "Material Properties and Compressive Local Buckling Response of High Strength Steel Square and Rectangular Hollow Sections." Engineering Structures 130 (January): 297–315. https://doi.org/10.1016/j.engstruct.2016.10.023.

Wang, Ying, Xiang Li, Tianyu Liao, Zhichao Lai, Chenxi Fang, and Junbo Zuo. 2024. "Axial Compressive Behavior of High-Strength Steel-UHPC-Clad Steel Composite Walls." Thin-Walled Structures 197 (April): 111588. https://doi.org/10.1016/j.tws.2024.111588.

Yao, Pengyu, Yuzhi Shi, Zhichao Lai, and Juntao Guo. 2025. "Experimental Test, Analysis, and Design of High-Strength SC Walls Subjected to Axial Compression." Journal of Structural Engineering 151 (4): 04025023. https://doi.org/10.1061/JSENDH.STENG-14108.

Zhang, Kai, Jungil Seo, and Amit H. Varma. 2020. "Steel-Plate Composite Walls: Local Buckling and Design for Axial Compression." Journal of Structural Engineering 146 (4): 04020044. https://doi.org/10.1061/(ASCE)ST.1943-541X.0002545.

Zhang, Kai, Amit H. Varma, Sanjeev R. Malushte, and Stewart Gallocher. 2014. "Effect of Shear Connectors on Local Buckling and Composite Action in Steel Concrete Composite Walls." Nuclear Engineering and Design 269 (April): 231–39. https://doi.org/10.1016/j.nucengdes.2013.08.035.